J. Fluid Mech. (2001), *vol.* 434, *pp.* 153–166. Printed in the United Kingdom

© 2001 Cambridge University Press

Diffuse-interface modelling of thermocapillary flow instabilities in a Hele-Shaw cell

By M. VERSCHUEREN, F. N. VAN DE VOSSE AND H. E. H. MEIJER

Material Technology, Dutch Polymer Institute, Eindhoven University of Technology, P.O. Box 513, 5600MB Eindhoven, The Netherlands

(Received 13 September 1999 and in revised form 6 November 2000)

In this paper we present the results of a diffuse-interface model for thermocapillary or Marangoni flow in a Hele-Shaw cell. We use a Galerkin-type spectral element discretization, based on Gauss–Lobatto quadrature, for numerical implementation of the governing equations resulting from the diffuse-interface model. The results are compared to classical results for a linear and circular fixed interface. It is found that the diffuse-interface solution converges to the classical solution in the sharp-interface limit. The results are sufficiently accurate if the interfacial thickness is only small compared to the size of the thermocapillary boundary layer, even if the interfacial thickness used is much larger than the real interfacial thickness. We also consider freely movable interfaces with a temperature gradient perpendicular to the interface. It will be shown that this situation can lead to a destabilizing Marangoni convection.

1. Introduction

An imposed temperature gradient along an interface between immiscible fluids can induce a flow if the interfacial tension depends on temperature. This phenomenon is called thermocapillary or Marangoni flow (Davis 1987) and is often encountered in industrial processing (Edwards, Brenner & Wassan 1991). In industrial processes thermocapillary flow is often accompanied by other phenomena which involve topological changes in interfaces, such as coalescence, break-up and phase separation (Kuhlmann 1999). In general, interfacial tension depends not only on temperature. It can also depend strongly on the concentration of a foreign component at the interface. This situation can lead to spontaneous interfacial activity, called 'interfacial turbulence' by Sternling & Scriven (1959). In some cases the interfacial deformation is so strong that droplets pinch off (Sherwood & Wei 1957). The goal of the present paper is to find a physical model and an appropriate numerical implementation which can describe thermocapillary flow allowing for topological changes.

In the classical approach to multi-component flow, an interface is assumed to be sharp and appropriate boundary conditions are applied to connect the various components. Solving the equations of fluid dynamics therefore involves solving a moving boundary problem. The most 'natural' numerical technique in this case is the tracking method (Hyman 1984; Unverdi & Tryggvason 1992): the discretization is such that grid points follow the interface. In the case of topological changes, however, the tracking method is inconvenient, since complicated re-meshing is necessary. To overcome this problem, Brackbill, Kothe & Zemach (1991) developed a continuum surface force (CSF) method in which the sharp interface is replaced by an artificial,

https://doi.org/10.1017/S0022112001003561 Published online by Cambridge University Press

continuous colour function. This colour function is used to determine the position and the geometry of the interface. Interfacial tension can now be included in the equation of motion as a body force. A direct application of boundary conditions is no longer required in this case and a fixed-grid numerical method can be used, which is convenient in the case of topological changes. The disadvantage of the CSF method is that the colour function is an arbitrary function, for which the interfacial thickness does not have a clear physical meaning. It has been shown that numerical results are sensitive to the choice of this colour function (Lowengrub & Truskinovsky 1998).

In diffuse-interface theories, which go back to the ideas of van der Waals (1979), the interface also has a non-zero thickness, but it is no longer arbitrary. It is determined by the molecular force balance at the interface and its value is closely related to the finite range of molecular interactions (Rowlinson & Widom 1989). Thermodynamically, the finite interaction range is represented by a non-local effect in the free energy: the local free energy density depends not only on the local composition, but also on the composition of the immediate environment (Davis & Scriven 1982). Cahn & Hilliard (1958) used a Taylor expansion of the free energy density about the homogeneous system. In this way, the non-local effect is represented by a dependence on local composition gradients rather than non-local composition. Non-classical expressions for the chemical potential and the stress tensor can then be derived in differential form. This allows a direct coupling with the equations of fluid dynamics.

The Cahn–Hilliard approach was originally designed to model spinodal decomposition (Cahn & Hilliard 1958). The diffuse-interface approach also allows the inclusion of hydrodynamic coupling: Gurtin, Polignone & Viñals (1996) used the diffuse-interface approach to study coarsening effects in binary fluids with hydrodynamic coupling and Anderson, McFadden & Wheeler (2000) used it to investigate solidification with convection. The diffuse-interface approach has also been used to study a wide range of hydrodynamic phenomena in which the fluids are thermodynamically in equilibrium: e.g. hydrodynamic instabilities (Lowengrub *et al.* 1998), mixing (Chella & Viñals 1996), break-up and moving contact lines (Jacqmin 1996, 2000). A review on recent developments in diffuse-interface modelling is given by Anderson, McFadden & Wheeler (1998). Antanovskii (1995) studied thermocapillary flow in the one-dimensional case using the diffuse-interface approach and Jasnow & Viñals (1996) studied thermocapillary motion of small droplets. Jasnow & Viñals also derived the sharp-interface expression for interfacial tension (gradients) from their diffuse-interface capillary term in the momentum equation, but they only show results for very small droplets. In this paper we focus on the question of whether the diffuse-interface model can be applied to droplets with radii much larger than the physical interfacial thickness.

In this paper we study thermocapillary motion in a Hele-Shaw cell. The results for fixed planar and circular interfaces are directly compared to the analytical results of Boos & Thess (1997). The dependence on the interfacial thickness is investigated, considering the sharp-interface limit. Finally, we study thermocapillary instabilities caused by a temperature gradient perpendicular to the interface. Section 2 is devoted to the classical, sharp-interface formulation of the problem. In § 3 the diffuse-interface theory is presented and non-classical expressions for the diffusion flux and the reversible part of the stress tensor are derived, following the principles of classical irreversible thermodynamics (de Groot & Mazur 1984). Section 4 is devoted to the numerical implementation of the governing equations, focusing on the Gauss–Lobatto spectral element discretization. Results are presented and discussed in §§ 5 and 6. Finally, § 7 contains some conclusions.

https://doi.org/10.1017/S0022112001003561 Published online by Cambridge University Press

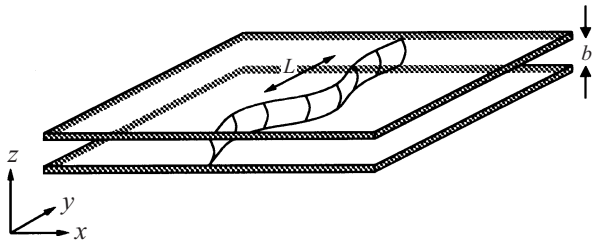


FIGURE 1. Schematic picture of a Hele-Shaw geometry, where b is the distance between the plates and L is the structure size of the interface.

2. System definition

Before moving on to the diffuse-interface formulation in the next section, we first present the classical, sharp-interface version of the problem. We consider two immiscible, incompressible, non-wetting fluids in a Hele-Shaw cell, which consists of two closely spaced parallel plates (see figure 1). We assume the two fluids to have equal density ρ and shear viscosity η. Along both plates, which are assumed to have a large thermal conductivity, a temperature gradient of the following form is imposed:

$$T = T_o + A\hat{\boldsymbol{e}}_T \cdot \boldsymbol{r}, \tag{2.1}$$

where A is a constant, $\hat{\boldsymbol{e}}_T$ is the unit vector in the direction of the temperature gradient and $\boldsymbol{r} = (x, y)$ is the spatial coordinate parallel to the plates. Interfacial tension γ is assumed to be a function of the temperature. For most fluids interfacial tension decreases with increasing temperature. We assume that the thermal Péclet number is small, that is $Pe_T = Vb/\lambda \ll 1$, where V is the thermocapillary velocity scale and λ is the heat diffusivity of the fluid. In this case the effect of fluid motion on the temperature field can be neglected, which means that the temperature of the fluid between the plates is also given by equation (2.1). It can be shown that, even if the heat diffusivity of the fluid is zero, the deviation from the plate temperature T is still small as long as the temperature gradient A and the plate spacing b are small (Boos & Thess 1997).

For small Reynolds numbers $Re = Vb/\nu$, with $\nu = \eta/\rho$ the kinematic viscosity, fluid flow is governed by the Stokes equations, which are in dimensionless form

$$\nabla^{(3)} \cdot \boldsymbol{v}^{(3)} = 0, \tag{2.2}$$

$$\nabla^{(3)} \cdot \boldsymbol{\tau}^{(3)} = \boldsymbol{0}, \tag{2.3}$$

where $\nabla^{(3)} = (\partial/\partial x, \partial/\partial y, \partial/\partial z)$, $\boldsymbol{v}^{(3)}$ is the three-dimensional velocity and $\boldsymbol{\tau}^{(3)} = -p^{(3)}\boldsymbol{I} + \nabla^{(3)}\boldsymbol{v} + \nabla^{(3)}\boldsymbol{v}^{\mathrm{T}}$ is the stress tensor, with $p^{(3)}$ the pressure, $\boldsymbol{I}$ the unit dyad. The kinematic and the stress boundary conditions are

$$[\![\boldsymbol{v}^{(3)}]\!] = 0, \tag{2.4}$$

$$[\![\boldsymbol{\tau}^{(3)} \cdot \hat{\boldsymbol{n}}]\!] = \frac{1}{Ca}(\gamma\hat{\boldsymbol{n}}\nabla_s^{(3)} \cdot \hat{\boldsymbol{n}} - \nabla_s^{(3)}\gamma), \tag{2.5}$$

respectively, where $Ca = \nu V/\gamma_o$ is the capillary number, $\hat{\boldsymbol{n}}$ is the unit vector normal to the interface and $\nabla_s^{(3)} = (\boldsymbol{I} - \hat{\boldsymbol{n}}\hat{\boldsymbol{n}}) \cdot \nabla^{(3)}$ denotes the interface gradient.

For non-wetting fluids in a Hele-Shaw geometry with small plate spacing b the bulk flow is a Poiseuille flow. In this case the three-dimensional governing equations can be averaged over the gap. This yields the following set of two-dimensional governing

https://doi.org/10.1017/S0022112001003561 Published online by Cambridge University Press

equations:

$$\nabla \cdot \boldsymbol{v} = 0, \tag{2.6}$$

$$\nabla p = \nabla^2 \boldsymbol{v} - k^2 \boldsymbol{v}, \tag{2.7}$$

where $\nabla = (\partial/\partial x, \partial/\partial y)$, $\boldsymbol{v} = (v_x, v_y)$ is the velocity averaged over the gap and $k = 12L^2/b^2$ is the dimensionless permeability of the cell. Equation (2.7) is the two-dimensional Stokes equation with an additional Darcy term, which takes into account the friction force of the flow due to the plates. The Darcy term is normally assumed to be much larger than the Stokes term. However, this approximation is only valid if the structure size L is much larger than the plate spacing and if the velocity gradients parallel to the plates are small compared to velocity gradients perpendicular to the plates. In case of thermocapillary flow, velocity gradients parallel to the plates can be large in a small region near the interface.

We assume that Stokes–Darcy equation (2.7) also applies to the interface and we will not consider any small-scale flow phenomena in the vicinity of the contact lines. (Jacqmin (1996, 2000) studied fluid motion near a moving contact line, using the diffuse-interface approach.) The contact lines are assumed to be either fixed or freely movable. In case of fixed contact lines the normal component of the kinematic boundary condition is $\boldsymbol{v} \cdot \hat{\boldsymbol{n}} = 0$.

The need to apply boundary conditions (2.4) and (2.5) is very inconvenient in the case of large interfacial deformations or topological changes in the interface. Furthermore, the physical mechanism controlling topological changes is missing. In the next section we present the diffuse-interface theory, which includes the physical mechanism by considering non-local effects in the free energy of the system. All properties vary continuously across the interface, which allows us to include interfacial tension as a locally acting body force.

3. Diffuse-interface theory

Diffuse-interface theories are based on non-local effects in the free energy of the system. As stated in the first section, these non-local effects can be represented by a dependence on local composition gradients. Therefore we start with the assumption that the specific internal energy u depends not only on the entropy s and the mass fraction of one of the components c, but also on the gradient of c. That is $u = u(s, c, \nabla c)$. Besides the continuity equation and the modified Stokes equation, where we use the term 'modified' because in the diffuse-interface approach the Stokes equation includes interfacial tension, we now also need the local balance equations for c, u and s (in this section we will omit the superscript $^{(3)}$ for three-dimensional systems). Hence, the set of governing equations now is

$$\nabla \cdot \boldsymbol{v} = 0, \tag{3.1}$$

$$\rho \frac{\mathrm{d}c}{\mathrm{d}t} = -\nabla \cdot \boldsymbol{j}, \tag{3.2}$$

$$\nabla \cdot \boldsymbol{\tau} = \boldsymbol{0}, \tag{3.3}$$

$$\rho \frac{\mathrm{d}u}{\mathrm{d}t} = \boldsymbol{\tau} : \nabla \boldsymbol{v} - \nabla \cdot \boldsymbol{q}, \tag{3.4}$$

$$\rho \frac{\mathrm{d}s}{\mathrm{d}t} = -\nabla \cdot \boldsymbol{j}_s + \sigma, \tag{3.5}$$

https://doi.org/10.1017/S0022112001003561 Published online by Cambridge University Press

where $\mathrm{d}/\mathrm{d}t = \partial/\partial t + \boldsymbol{v}\cdot\nabla$, $\boldsymbol{j}$ is the diffusion flux, $\boldsymbol{q}$ is the energy flux, $\boldsymbol{j}_s$ is the entropy flux and σ is the entropy production. The second law of thermodynamics states that we must have $\sigma \geqslant 0$, where the equal sign applies for systems in equilibrium or reversible changes. In the diffuse-interface approach the stress tensor $\boldsymbol{\tau}$ also includes interfacial tension and is, therefore, no longer defined by the classical relation given in § 2. One expects an additional reversible part, depending on ∇c, which includes interfacial tension as a body force. In a similar way, the diffusion flux $\boldsymbol{j}$ and the energy flux $\boldsymbol{q}$ also depend on ∇c.

To find relations for $\boldsymbol{j}$, $\boldsymbol{\tau}$ and $\boldsymbol{q}$, we follow the principles of classical irreversible thermodynamics (de Groot & Mazur 1984): the fluxes are assumed to be linear functions of the thermodynamic forces appearing in the entropy production σ. A more explicit expression for σ can be found by considering the Gibbs relation, which is given by the total differential of u. Assuming local equilibrium for a volume element moving with the flow (de Groot & Mazur 1984), the Gibbs relation is

$$\frac{\mathrm{d}u}{\mathrm{d}t} = \left.\frac{\partial u}{\partial s}\right|_{c,\nabla c}\frac{\mathrm{d}s}{\mathrm{d}t} + \left.\frac{\partial u}{\partial c}\right|_{s,\nabla c}\frac{\mathrm{d}c}{\mathrm{d}t} + \left.\frac{\partial u}{\partial \nabla c}\right|_{s,c}\cdot\frac{\mathrm{d}\nabla c}{\mathrm{d}t}. \tag{3.6}$$

In what follows we omit the subscripts denoting the variables which are kept constant. The local balance equation for ∇c can be found by considering the gradient of equation (3.2). After some manipulations we find

$$\frac{\mathrm{d}\nabla c}{\mathrm{d}t} = -\nabla\boldsymbol{v}\cdot\nabla c - \nabla\left(\frac{1}{\rho}\nabla\cdot\boldsymbol{j}\right). \tag{3.7}$$

Combining equations (3.2) to (3.7) we obtain the following relation for the entropy production:

$$\sigma = \frac{1}{T}(\boldsymbol{\tau}-\tilde{\boldsymbol{\tau}}):\nabla_d\boldsymbol{v} + (\boldsymbol{q}-\tilde{\boldsymbol{q}})\nabla\frac{1}{T} - \boldsymbol{j}\cdot\nabla\frac{\mu}{T}, \tag{3.8}$$

where $\nabla_d\boldsymbol{v}$ is the deviatoric part of $\nabla\boldsymbol{v}$ and

$$\tilde{\boldsymbol{\tau}} = -\rho\frac{\partial u}{\partial\nabla c}\nabla c, \tag{3.9}$$

$$\tilde{\boldsymbol{q}} = \rho\frac{\partial u}{\partial\nabla c}\nabla\cdot\boldsymbol{j}, \tag{3.10}$$

$$\mu = \frac{\partial u}{\partial c} - \nabla\cdot\frac{\partial u}{\partial\nabla c} \tag{3.11}$$

are the reversible part of the stress tensor, the energy flux due to mass diffusion and the generalized chemical potential, respectively. The entropy production has a simple structure: it is the sum of the products of the thermodynamic fluxes and forces. In equilibrium both fluxes and forces vanish. Consequently, the equilibrium parts of the diffusion and the energy flux are equal to zero and the reversible part of the stress tensor can be written as $\boldsymbol{\tau}_r = -p\boldsymbol{I} + \tilde{\boldsymbol{\tau}}$, where p is an arbitrary pressure field.

The dissipative parts of fluxes, the viscous stress tensor $\boldsymbol{\tau}_v = \boldsymbol{\tau} - \boldsymbol{\tau}_r$, the energy flux $\boldsymbol{q}$ and the diffusion flux $\boldsymbol{j}$, are assumed to be linear functions of the thermodynamic forces. Keeping in mind that fluxes and forces of different tensorial character do not couple, we obtain

$$\boldsymbol{\tau}_v = \frac{\Lambda_v}{2T}(\nabla\boldsymbol{v} + \nabla\boldsymbol{v}^{\mathrm{T}}), \tag{3.12}$$

https://doi.org/10.1017/S0022112001003561 Published online by Cambridge University Press

$$\boldsymbol{q} = -\Lambda_{qq}\nabla\frac{1}{T} - \Lambda_{qj}\nabla\frac{\mu}{T}, \tag{3.13}$$

$$\boldsymbol{j} = -\Lambda_{jq}\nabla\frac{1}{T} - \Lambda_{jj}\nabla\frac{\mu}{T}, \tag{3.14}$$

where we have assumed that the viscous stress tensor is symmetric. The Λ are the phenomenological coefficients. The coefficient $\Lambda_v/2T$ can be identified as the shear viscosity η, Λ_{qq}/T^2 is the heat conductivity and Λ_{jj} is the mobility parameter. Equations (3.13) and (3.14) also include the cross-effects, the Soret and the Dufour effect (Bird, Stewart & Lightfoot 1960), which will be neglected in what follows.

In this paper we are only concerned with small linear temperature gradients which do not change in time. In this case the governing equations are given by

$$\nabla\cdot\boldsymbol{v} = 0, \tag{3.15}$$

$$\rho\frac{\mathrm{d}c}{\mathrm{d}t} = \frac{\Lambda_{jj}}{T_o}\nabla^2\mu, \tag{3.16}$$

$$\nabla\cdot(\boldsymbol{\tau}_r + \boldsymbol{\tau}_v) = \boldsymbol{0}, \tag{3.17}$$

where we have assumed that Λ_{jj} is constant. To complete this set of equations we need an equation of state for the inhomogeneous system. Using a Taylor expansion about the homogeneous system, Cahn & Hilliard (1958) derived the following form for the specific Helmholtz free energy:

$$f(T,c,\nabla c) = f_h(T,c) + \tfrac{1}{2}\epsilon|\nabla c|^2, \tag{3.18}$$

where ϵ is the gradient energy parameter, which is assumed to be constant. Using an additional Taylor expansion of f_h about the critical temperature T_c and the critical composition c_c yields the Ginzburg–Landau form (Gunton, Miguel & Sahni 1983)

$$f(T,\tilde{c},\nabla\tilde{c}) = \tfrac{1}{4}\beta\tilde{c}^4 - \tfrac{1}{2}\alpha(T_c - T)\tilde{c}^2 + \tfrac{1}{2}\epsilon|\nabla\tilde{c}|^2, \tag{3.19}$$

where $\tilde{c} = c - c_c$. The parameters α and β are both positive constants. Using the thermodynamic relations $\partial u/\partial c|_{s,\nabla c} = \partial f/\partial c|_{T,\nabla c}$ and $\partial u/\partial\nabla c|_{s,c} = \partial f/\partial\nabla c|_{T,c}$ the chemical potential (3.11) can be written as

$$\mu = \beta c^3 - \alpha(T_c - T)c - \epsilon\nabla^2 c, \tag{3.20}$$

where we have omitted the tilde notation. At equilibrium μ equals zero. Besides the spatially uniform (bulk) solutions $c = \pm c_B$, with $c_B = \sqrt{\alpha(T_c - T)/\beta}$, there is another possible solution, which represents the interface profile. For a planar interface, with z the direction normal to the interface, this solution is given by

$$c = c_B\tanh\frac{z}{\sqrt{2}\xi} \quad \text{with} \quad \xi = \sqrt{\frac{\epsilon}{\alpha(T_c - T)}}, \tag{3.21}$$

where ξ is the interfacial thickness.

Interfacial tension γ is determined by the choice of the equation of state. It can be defined as the excess tangential stress:

$$\gamma = \int_{-\infty}^{\infty}\hat{\boldsymbol{n}}\cdot(\boldsymbol{\tau}_r\cdot\hat{\boldsymbol{n}} - \boldsymbol{\tau}_r\cdot\hat{\boldsymbol{t}})\mathrm{d}z = \rho\epsilon\int_{-\infty}^{\infty}(\mathrm{d}c/\mathrm{d}z)^2\mathrm{d}z. \tag{3.22}$$

Using equation (3.21) we obtain

$$\gamma = \frac{2\sqrt{2}}{3}\frac{\rho\sqrt{\epsilon}}{\beta}[\alpha(T_c - T)]^{3/2}. \tag{3.23}$$

https://doi.org/10.1017/S0022112001003561 Published online by Cambridge University Press

In the momentum equation interfacial tension is included in $\nabla \cdot \boldsymbol{\tau}_r$. For small temperature gradients $\nabla \cdot \boldsymbol{\tau}_r$ can be rewritten as $\nabla \cdot \boldsymbol{\tau}_r = -\nabla \rho g + \rho \mu \nabla c$, where $g = f + p/\rho$ is the specific Gibbs free energy. The momentum equation can then be written as (from now the equations are two-dimensional)

$$\nabla g = \nu(\nabla^2 \boldsymbol{v} - k^2 \boldsymbol{v}) + \mu \nabla c, \tag{3.24}$$

where we used the Stokes–Darcy approximation for the viscous part. Computationally, it is convenient to rewrite the momentum equation in terms of the stream function ψ, which is defined by $\boldsymbol{v} = (\partial\psi/\partial y, -\partial\psi/\partial x)$. In this way mass conservation is automatically satisfied. The equation for ψ is found by taking the curl of equation (3.24). This yields

$$\nu \nabla^2(\nabla^2 \psi - k^2 \psi) = \nabla \times \mu \nabla c, \tag{3.25}$$

where $\nabla\times$ denotes the curl.

To scale the governing equations we use the following dimensionless variables: $c^* = c/c_{Bo}$, $\boldsymbol{r}^* = \boldsymbol{r}/L$, $\boldsymbol{v}^* = \boldsymbol{v}/V$, $\mu^* = \mu\xi_o^2/(\epsilon c_{Bo})$, $t^* = tV/L$, $T^* = T/T_o$ and $\psi^* = \psi/(LV)$, where $\xi_o = \xi(T_o)$ and $c_{Bo} = c_B(T_o)$. Omitting the asterisk notation we obtain the following dimensionless governing equations:

$$\frac{\mathrm{d}c}{\mathrm{d}t} = \frac{1}{Pe}\nabla^2 \mu \quad \text{with } \mu = c^3 - (1 - \zeta \hat{\boldsymbol{e}}_T \cdot \boldsymbol{r})c - C^2 \nabla^2 c, \tag{3.26}$$

$$\nabla^2(\nabla^2 \psi - k^2 \psi) = \frac{1}{Ca}\frac{1}{C}\nabla \times \mu \nabla c, \tag{3.27}$$

where the Péclet number Pe, the temperature parameter ζ, the capillary number Ca and the dimensionless interfacial thickness C, called Cahn number in the rest of this paper, are given by

$$Pe = \frac{\rho T_o \xi_o^2 LV}{\Lambda_{jj}\epsilon}, \quad \zeta = \frac{AL}{T_c - T_o}, \quad Ca = \frac{\xi_o \nu V}{\epsilon c_{Bo}^2} \quad \text{and} \quad C = \frac{\xi_o}{L}, \tag{3.28}$$

respectively. In the classical approach the set of dimensionless parameters looks different: Pe and C are absent and the capillary number is defined as $Ca_{\mathrm{cl}} = \eta V/\gamma_o$. Using equation (3.23) the capillary number can be rewritten as $Ca = \frac{2}{3}\sqrt{2}\,\eta V/\gamma_o$, where $\gamma_o = \gamma(T_o)$. This shows that $Ca/Ca_{\mathrm{cl}} = \frac{2}{3}\sqrt{2}$.

Analytical solutions can only be obtained in some special cases. In general a numerical implementation is needed.

4. Computational methods

To discretize the governing equations we use a spectral element method (Timmermans, van de Vosse & Minev 1994). The basis functions ϕ, which are used for the spatial discretization, are high-order Lagrange interpolation polynomials through the Gauss–Lobatto integration points defined per element.

The momentum equation (3.24) is a fourth-order differential equation in ψ. Since the basis functions ϕ are elements of H^1, that is $H^1(\Omega) = \{\phi \mid \phi \in L^2(\Omega), \nabla\phi \in L^2(\Omega) \times L^2(\Omega)\}$, we split the momentum equation into two second-order differential equations

$$\nabla^2 Q = h, \tag{4.1}$$

$$\nabla^2 \psi - k^2 \psi = Q, \tag{4.2}$$

where $h = Ca^{-1}C^{-1}\nabla \times \mu \nabla c$. The boundary conditions for Q and ψ are either

https://doi.org/10.1017/S0022112001003561 Published online by Cambridge University Press

homogeneous Neumann or Dirichlet. The Galerkin weighted-residual representation of the differential equations is

$$(\nabla^2 Q, w)_\Omega = (h, w)_\Omega, \tag{4.3}$$

$$(\nabla^2 \psi, w)_\Omega - k^2(\psi, w)_\Omega = (Q, w)_\Omega, \tag{4.4}$$

where the inner product $(a, w)_\Omega = \int_\Omega a w \mathrm{d}^2\boldsymbol{r}$ and w is the standard Galerkin test function. Partial integration of the integrals on the left-hand side yields the weak or variational form

$$-(\nabla Q, \nabla w)_\Omega = (h, w)_\Omega, \tag{4.5}$$

$$-(\nabla \psi, \nabla w)_\Omega - k^2(\psi, w)_\Omega = (Q, w)_\Omega, \tag{4.6}$$

where the boundary integrals vanish because of the homogeneous boundary conditions. The next step is to decompose the total domain Ω in N_{el} non-overlapping sub-domains Ω_e and apply the spectral discretization on each element:

$$\boldsymbol{Q}^e = \sum_{l,m=1}^{N} Q^e_{lm} \tilde{\phi}^e_{lm}, \tag{4.7}$$

where $\tilde{\phi}_{lm}$ is the two-dimensional Lagrange interpolation function through the Legendre–Gauss–Lobatto integration points ($l, m = 1 \ldots N$), which is the tensor product of the one-dimensional interpolation functions: $\tilde{\phi}_{lm} = \phi_l \phi_m$. Using similar discretizations for ψ, w and f and assembling the elements we obtain the following discrete set of equations:

$$\boldsymbol{S}\boldsymbol{Q} = \boldsymbol{M}\boldsymbol{h}, \tag{4.8}$$

$$\boldsymbol{S}\boldsymbol{\psi} - k^2\boldsymbol{M}\boldsymbol{\psi} = \boldsymbol{M}\boldsymbol{Q}, \tag{4.9}$$

where $\boldsymbol{S}$ is the diffusion matrix, $\boldsymbol{M}$ is the mass matrix and $\boldsymbol{Q}$, $\boldsymbol{h}$ and $\boldsymbol{\psi}$ are the discrete vector representations of Q, h and ψ, respectively. The results presented in §§ 5 and 6 were all obtained using a fixed mesh with seventh-order quadrilateral spectral elements.

The composition equation and the equation for the chemical potential are also a set of two second-order differential equations, which we will solve in a coupled way. Besides spatial discretization we now also need temporal discretization. Using the Euler implicit method for time discretization and the same spatial discretization as for the momentum equation we obtain

$$\begin{bmatrix} \boldsymbol{M} - \Delta t \boldsymbol{N}^n & \dfrac{\Delta t}{Pe}\boldsymbol{S} \\ [1 - \zeta \hat{\boldsymbol{e}}_{T\cdot\boldsymbol{r}} - (\boldsymbol{c}_i^{n+1})^2]\boldsymbol{M} - C^2\boldsymbol{S} & \boldsymbol{M} \end{bmatrix} \begin{bmatrix} \boldsymbol{c}_{i+1}^{n+1} \\ \boldsymbol{\mu}_{i+1}^{n+1} \end{bmatrix} = \begin{bmatrix} \boldsymbol{M}\boldsymbol{c}_0^n \\ 0 \end{bmatrix}, \tag{4.10}$$

where $\boldsymbol{M}$ is the mass matrix, $\boldsymbol{N}$ is the convection matrix with $\boldsymbol{v} = (\partial\psi/\partial y, -\partial\psi/\partial x)$ and $\boldsymbol{S}$ is the diffusion matrix. Superscript n denotes time t and $n+1$ denotes $t+\Delta t$. A Picard iteration is used to deal with the nonlinear term (subscript $i = 1 \ldots I$): the iteration starts using $\boldsymbol{c}_I^{n+1} = \boldsymbol{c}_0^n$ and as a stopping criterion we use $\max|\boldsymbol{c}_{I+1}^{n+1} - \boldsymbol{c}_1^{n+1}| < 10^{-4}$. After convergence, $\boldsymbol{\mu}_{I+1}^{n+1}$ and $\boldsymbol{c}_{I+1}^{n+1}$ are used to compute a new h and we can move to the next time step.

https://doi.org/10.1017/S0022112001003561 Published online by Cambridge University Press

5. Classical vs. diffuse-interface results

In this section we compare our computational diffuse-interface results for thermocapillary flow with classical analytical results of Boos & Thess (1997) for fixed planar and circular interfaces. We investigate how the results depend on the Cahn number C.

To be able to make a direct comparison with the classical results we have to make sure that we use the same assumptions and the same scaling. In their paper Boos & Thess assumed that γ is a linear function of temperature. That is

$$\gamma = \gamma_o - B(T - T_o), \tag{5.1}$$

where B is a positive constant. In our case, interfacial tension is given by equation (3.23), which is nonlinear in T. However, for small values of ζ, defined in (3.28), we can approximate γ as

$$\gamma = \frac{2\sqrt{2}}{3}\frac{\rho\epsilon}{\xi_o}c_{Bo}^2(1 - \tfrac{3}{2}\zeta\hat{\boldsymbol{e}}_T \cdot \boldsymbol{r}^*). \tag{5.2}$$

In this way we find

$$B = \frac{\mathrm{d}\gamma}{\mathrm{d}T} = \frac{1}{AL}\frac{\mathrm{d}\gamma}{\mathrm{d}\hat{\boldsymbol{e}}_T \cdot \boldsymbol{r}^*} = \sqrt{2}\frac{\rho\epsilon}{\xi_o}c_{Bo}^2\frac{1}{T_c - T_o}. \tag{5.3}$$

Boos & Thess used $V = \frac{1}{2}ABL/\eta$ as the velocity scale. In our case this yields

$$Ca = \tfrac{1}{2}\sqrt{2}\,\zeta. \tag{5.4}$$

For small temperature gradients we can also approximate the composition profile c by the equilibrium profile at $T = T_o$, that is $c = c_o = c(T_o)$. With these approximations the momentum equation is

$$\nabla^2(\nabla^2\psi - k^2\psi) = \frac{\sqrt{2}}{\zeta C}\nabla \times \mu\nabla c_o, \tag{5.5}$$

with μ given by equation (3.26).

First we will consider a planar, fixed interface with a temperature gradient parallel to it, as schematically depicted in figure 2(*a*). The direction of the temperature gradient is indicated by the arrow. In the absence of a lateral length scale we have chosen $L = b$ and consequently $k = \sqrt{12}$. The temperature gradient induces an interfacial tension gradient in the opposite direction, which causes stretching of the interface at higher temperatures and shrinkage at lower temperature. This process also induces a velocity in the surrounding fluid. Figure 2(*b*) shows the classical and the diffuse-interface results for this thermocapillary flow. The diffuse-interface result for $k = \sqrt{12}$, $\zeta = \sqrt{2}$, and $C = 0.1, 0.05, 0.01, 0.005$ are shown. The corresponding classical result is $v_x(y) = -\exp(-\sqrt{12}y)/\sqrt{12}$. The diffuse-interface results were obtained by solving equation (5.5) with $c_o = \tanh((y+1)/(\sqrt{2}C))$. The inset in figure 2(*b*) shows the flow near the interface in more detail. The results show a clear convergence to the classical solution for $C \to 0$.

The second case we consider is thermocapillary flow in and outside a circular droplet with a fixed interface, as depicted in figure 3. The radius of the droplet is used as the length scale. The temperature gradient again causes stretching at $x = 1$ and shrinkage at $x = -1$. This will induce a flow in and outside the droplet with a streamline pattern as shown in figure 4. The classical (*a*) and the diffuse-interface results (*b*) for the streamline pattern are shown for $k = 2\sqrt{12}$ and $k = 20\sqrt{12}$, where we used

https://doi.org/10.1017/S0022112001003561 Published online by Cambridge University Press

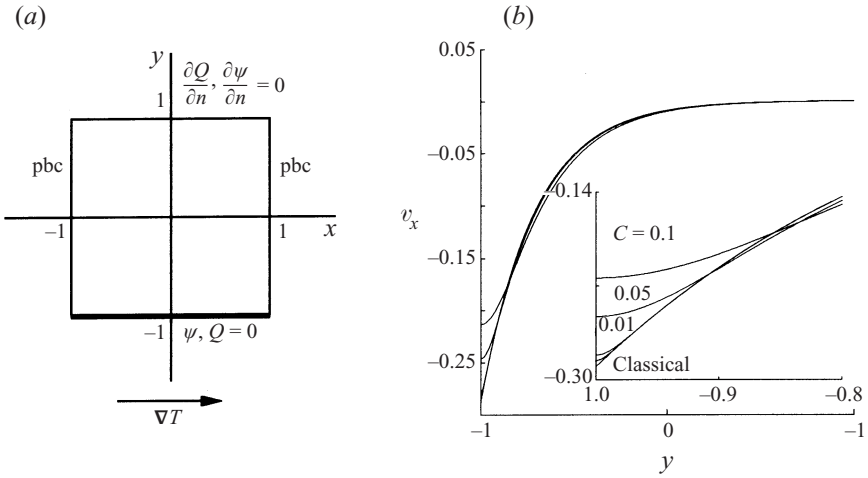


FIGURE 2. (*a*) Planar interface, located at $y = -1$, with a temperature gradient parallel to it and (*b*) the resulting thermocapillary flow: classical and diffuse-interface for $k = \sqrt{12}$, $\zeta = \sqrt{2}$, $C = 0.1, 0.05, 0.01, 0.005$.

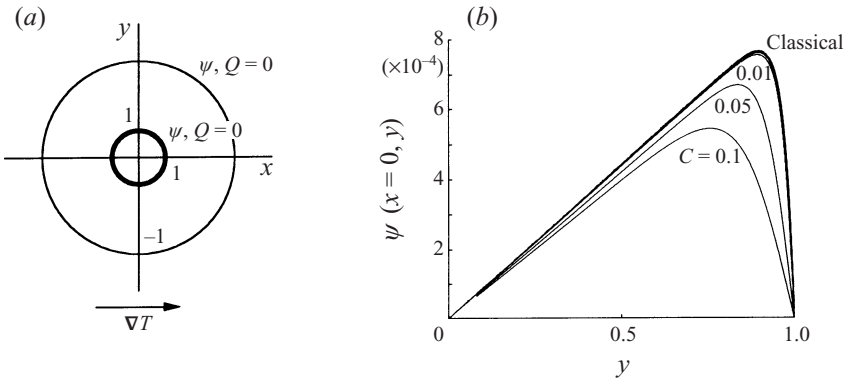


FIGURE 3. (*a*) Circular droplet with a temperature gradient in the *x*-direction and (*b*) the results for the thermocapillary flow: classical and diffuse-interface for $k = 10\sqrt{12}$, $\zeta = \sqrt{2}$, $C = 0.1, 0.05, 0.01, 0.005, 0.001$.

$C = 0.01$ and $\zeta = \sqrt{2}$. The pattern inside the droplet matches the classical result. The pattern outside the droplet differs from the classical result, because the classical results were obtained on an infinite domain whereas we used a finite domain for the diffuse-interface calculations. Therefore, the flow field far away from the droplet is different, but the flow field in the vicinity of the droplet matches the classical result. Figure 3(*b*) shows ψ inside the droplet for $x = 0, 0 \leqslant y \leqslant 1$, where we used $k = 10\sqrt{12}$. The classical result and the diffuse-interface results for $C = 0.1, 0.05, 0.01, 0.005, 0.001$ are shown. Again, we find a clear convergence to the classical solution for $C \to 0$. There is a good match if C is smaller than the thermocapillary boundary layer $\delta \sim k^{-1}$.

In this section we have only considered fixed interfaces. If the contact lines of the droplet were freely movable the droplet would migrate towards higher temperatures. This process was investigated by Jasnow & Viñals (1996). In the next section we will

https://doi.org/10.1017/S0022112001003561 Published online by Cambridge University Press

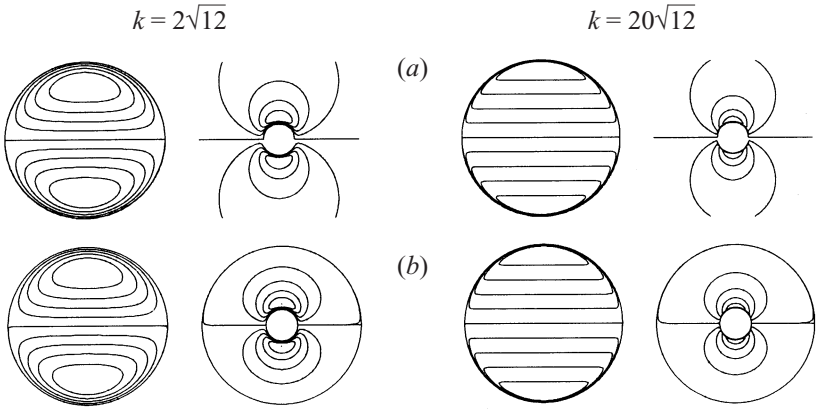


FIGURE 4. (*a*) Classical results and (*b*) diffuse-interface results for the flow field in and outside the droplet for $k = 2\sqrt{12}$ and $k = 20\sqrt{12}$. In both cases $C = 0.01$ and $\zeta = \sqrt{2}$ was used.

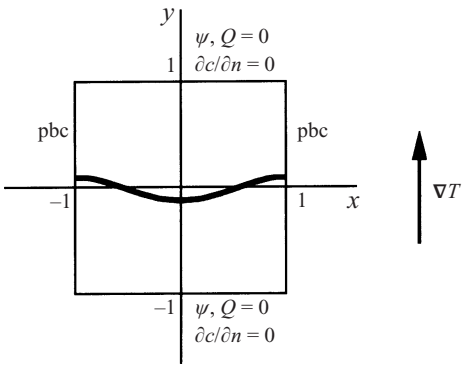


FIGURE 5. A perturbed interface with a temperature gradient perpendicular to it.

consider a freely movable interface with a temperature gradient perpendicular to it and we investigate how this affects the stability of the interface.

6. Thermocapillary instabilities

Consider an interface with a temperature gradient perpendicular to it as depicted in figure 5. A small perturbation in the interface towards the high temperature side now leads to local stretching of the interface. We shall see that this can lead to a destabilizing Marangoni convection.

In the diffuse-interface approach interfacial tension is fixed by the choice of the equation of state. Therefore, we can only vary the interfacial tension by varying temperature. However, the dependence of interfacial tension on temperature can be different for another choice of fluids. We now assume that the momentum equation for other systems can still be written in the form of equation (5.5), but we replace ζ by an independent parameter $\tilde{\zeta}$. This way we can choose the ratio of the interfacial tension gradients and interfacial tension independent of the temperature gradient. Choosing ζ small compared to $\tilde{\zeta}$ means that temperature effects relate exclusively to interfacial tension. Assuming that ζ is small, we can now write the governing

https://doi.org/10.1017/S0022112001003561 Published online by Cambridge University Press

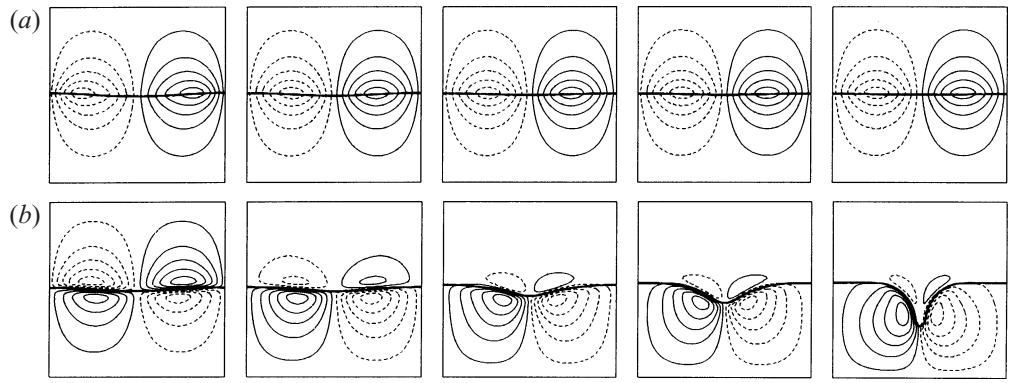


FIGURE 6. Time development ($t = 0, 150, 250, 400, 500$) of a perturbed interface with a temperature gradient perpendicular to it for $\tilde{\zeta} = 0.1$ (*a*) and for $\tilde{\zeta} = 10$ (*b*). We used $k = 10\sqrt{12}$, $Pe = 10^4$ and $C = 0.01$. The streamlines are also shown: for the solid lines the motion is clockwise and for the dashed lines counterclockwise.

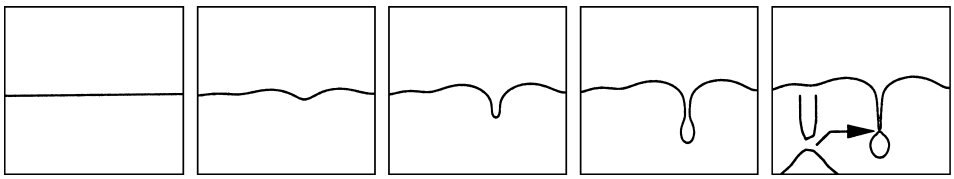


FIGURE 7. Time sequence ($t = 0, 740, 800, 830, 850$) of a randomly perturbed interface with a temperature gradient perpendicular to it for $\tilde{\zeta} = 20$, $k = 10\sqrt{12}$, $Pe = 10^4$ and $C = 0.01$.

equations as

$$\frac{\mathrm{d}c}{\mathrm{d}t} = \frac{1}{Pe}\nabla^2\mu_o, \tag{6.1}$$

$$\nabla^2(\nabla^2\psi - k^2\psi) = \frac{\sqrt{2}}{\tilde{\zeta}C}\nabla\times(\mu_o + \tilde{\zeta}yc)\nabla c. \tag{6.2}$$

One of the advantages of this choice of the governing equations is that we can use simple homogeneous Neumann boundary conditions, that is $\partial c/\partial n = 0$, to ensure mass conservation.

Figure 6 shows the time development of an interface with an initial perturbation as depicted in figure 5 for two values of $\tilde{\zeta}$. For $\tilde{\zeta} = 0.1$ the interfacial tension gradients are too weak compared to the interfacial tension itself and a stabilizing motion sets in. For $\tilde{\zeta} = 10$ the interfacial tension gradients dominate and the perturbation grows. For larger values of k the system would be unstable for smaller values of $\tilde{\zeta}$, but the thermocapillary boundary layer is more difficult to capture for large values of k since we have to use $C < k^{-1}$ to obtain the correct results.

The observed instability is different from Rayleigh–Bénard instabilities (Davis 1987), since we did not include heat convection due to fluid motion. Heat convection would have a stabilizing effect on the instability shown in figure 6: the convection cells would transport low temperature to regions of low tension and high temperature to regions of high tension.

Finally, we show the time development of a planar interface with small random perturbation (see figure 7). The resulting instability is similar to the one observed in

https://doi.org/10.1017/S0022112001003561 Published online by Cambridge University Press

figure 6. The interfacial deformation is so strong that a droplet pinches off. Strong interfacial deformations as in figure 6 were also observed in other systems with low interfacial tension and high interfacial tension gradients. For example, adding a small amount of solvent to the binary system can induce large interfacial tension gradients if the interfacial tension depends strongly on the solvent concentration. This situation can lead to what Sternling & Scriven have called 'interfacial turbulence' (Sherwood & Wel 1957; Sternling & Scriven 1959). Also some polymer–solvent–nonsolvent systems, in which interfacial tension depends strongly on the solvent concentration, show this kind of interfacial deformation, often referred to as macrovoid formation (Berghmans 1995). A direct qualitative comparison between 'interfacial turbulence' and the instability observed in figure 6 is difficult because in the three-component system there is convection of the solvent component, whereas in our case there is no temperature convection. However, in both cases the instability is caused by the fact that interfacial tension is small and interfacial tension gradients are large.

Figure 6 also shows that we can also handle topological changes in the interface. However, the pinch-off also introduces another length scale, which is related to the thickness of the drainage layer before pinch-off. This length scale is often smaller than the size of thermocapillary boundary layer. Furthermore, as soon as the drainage layer size becomes smaller than the distance b between the plates the Hele-Shaw formulation of the problem breaks down and it becomes essentially a three-dimensional problem. To get correct results for the pinch-off we have to choose C such that the diffuse interface thickness is small compared to the size of the drainage layer. For too large values of C the pinch-off time will be underestimated (Lowengrub & Truskinovsky 1998).

7. Conclusions

In this paper we have presented the diffuse-interface approach to thermocapillary flow. A Galerkin-type spectral element discretization, based on Gauss–Lobatto quadrature, was used for numerical implementation of the governing equations. The high-order spectral interpolation is very suitable for an accurate capturing of small interfacial thicknesses (Verschueren, van de Vosse & Meijer 1998).

The computational results were compared directly to analytical classical results. The diffuse-interface result converges to the classical results for Cahn number $C \to 0$. The results shows that, to obtain a sufficiently accurate match with the sharp-interface result, we do not have to use the physical value for the interfacial thickness. Sufficiently accurate results were obtained when C is smaller than the thermocapillary boundary layer $\delta \sim k^{-1}$.

Finally, the effect of a temperature gradient perpendicular to an interface on the stability of the interface was investigated. The interface is unstable for systems in which forces due to interfacial tension gradients dominate interfacial tension forces. The results are in qualitative agreement with the linear stability analysis presented by Boos & Thess (1997). The results also show that the diffuse-interface model is very suitable for modelling instabilities causing large interfacial deformations and even topological changes. However, to obtain correct results in the case of droplet pinch-off C has to be such that the diffuse interface thickness is sufficiently smaller than the length scale typical for the drainage layer just before pinch-off. This length scale is often much smaller than the size of the thermocapillary boundary layer.

We would like to thank PTN (Polymeer Technologie Nederland) and DPI (Dutch Polymer Institute) for their financial support.

https://doi.org/10.1017/S0022112001003561 Published online by Cambridge University Press

REFERENCES

Anderson, D. M., McFadden, G. B. & Wheeler, A. A. 1998 Diffuse-interface methods in fluid mechanics. *Ann. Rev. Fluid Mech.* **30**, 139–165.

Anderson, D. M., McFadden, G. B. & Wheeler, A. A. 2000 A phase-field model of solidification with convection. *Physica* D **135**, 175–194.

Antanovskii, L. K. 1995 A phase-field model of capillarity. *Phys. Fluids* **7**, 747–753.

Berghmans, S. 1995 Spinning of hollow fibres. PhD thesis, Leuven, Belgium.

Bird, R. B., Stewart, W. E. & Lightfoot, E. N. 1960 *Transport Phenomena*. Wiley.

Boos, W. & Thess, A. 1997 Thermocapillary flow in a Hele-Shaw cell. *J. Fluid Mech.* **352**, 305–330.

Brackbill, J. U., Kothe, D. B. & Zemach, C. 1991 A continuum model for modeling surface tension. *J. Comput. Phys.* **100**, 335–354.

Cahn, J. W. & Hilliard, J. E. 1958 Free energy of a nonuniform system. I. Interfacial energy. *J. Chem. Phys.* **28**, 258–267.

Chella, R. & Viñals, J. 1996 Mixing of a two-phase fluid by cavity flow. *Phys. Rev.* E **53**, 3832–3840.

Davis, H. T. & Scriven, L. E. 1982 Stress and structure in fluid interfaces. *Adv. Chem. Phys.* **49**, 357–454.

Davis, S. H. 1987 Thermocapillary instabilities. *Ann. Rev. Fluid Mech.* **19**, 403–435.

Edwards, D. A., Brenner, H. & Wassan, D. T. 1991 *Interfacial Transport Processes and Rheology*. Butterworth Heinemann.

Groot, S. R. de & Mazur, P. 1984 *Non-Equilibrium Thermodynamics*. Dover.

Gunton, J. D., Miguel, M. S. & Sahni, P. S. 1983 *The Dynamics of First-Order Phase Transitions, Phase Transitions and Critical Phenomena*, vol. 8, Academic.

Gurtin, M. E., Polignone, D. & Viñals, J. 1996 Two-phase binary fluids and immiscible fluids described by an order parameter. *Math. Models Methods Appl. Sci.* **6**, 815.

Hyman, J. M. 1984 Numerical methods for tracking interfaces. *Physica* D **12**, 396–407.

Jacqmin, D. 1996 An energy approach to the continuum surface tension method. *AIAA Paper* 96-0858.

Jacqmin, D. 2000 Contact-line dynamics of a diffuse fluid interface. *J. Fluid Mech.* **402**, 57–88.

Jasnow, D. & Viñals, J. 1996 Coarse-grained description of thermo-capillary flow. *Phys. Fluids* **8**, 660–669.

Kuhlmann, H. C. 1999 *Thermocapillary Convection in Models of Crystal Growth*. Springer.

Lowengrub, J., Goodman, J., Lee, H., Longmire, E., Shelley, M. J. & Truskinovsky, L. 1998 Topological transitions in liquid/liquid interfaces. In *Proc. 1997 Intl Congress on Free Boundary Problems* (ed. I. Athanasopoulos, M. Makrakis & J. F. Rodrigues). Addison-Wesley Longman.

Lowengrub, J. & Truskinovsky, L. 1998 Quasi-incompressible Cahn Hilliard fluids. *Proc. R. Soc. Lond.* A **454**, 2617–2654.

Rowlinson, J. S. & Widom, B. 1989 *Molecular Theory of Capillarity*. Clarendon.

Sherwood, T. K. & Wei, J. C. 1957 Interfacial phenomena in liquid extraction. *Indust. Engng Chem.* **49**, 1030–1034.

Sternling, C. V. & Scriven, L. E. 1959 Interfacial turbulence: hydrodynamic instability and the Marangoni effect. *AIChE J.* **5**, 514–523.

Timmermans, L. J. P., Vosse, F. N. van de & Minev, P. D. 1994 Taylor-Galerkin-based spectral element methods for convection-diffusion problems. *Intl J. Numer. Meth. Fluids* **18**, 853–870.

Unverdi, S. O. & Tryggvason, G. 1992 Computations of multi-fluid flow. *J. Comput. Phys.* **60**, 70–83.

Verschueren, M., Vosse, F. N. van de & Meijer, H. E. H. 1998 A high order interface capturing technique for structure development in binary fluids. *ICOSAHOM'98, June 22–26, Herzliya, Israel*.

Waals, J. D. van der 1979 The thermodynamic theory of capillarity under the hypothesis of a continuous density variation. *J. Statist. Phys.* **20**, 197–244, translated by J. S. Rowlinson.

https://doi.org/10.1017/S0022112001003561 Published online by Cambridge University Press